

# Template-free synthesis of molybdenum oxide-based hierarchical microstructures at low temperatures

Liang Fang<sup>a,b</sup>, Yuying Shu<sup>a</sup>, Aiqin Wang<sup>a</sup>, Tao Zhang<sup>a,\*</sup>

<sup>a</sup> State Key Laboratory of Catalysis, Dalian Institute of Chemical Physics, Chinese Academy of Sciences, Dalian 116023, China

<sup>b</sup> Graduate School of the Chinese Academy of Sciences, Beijing 100049, China

## ARTICLE INFO

### Article history:

Received 12 March 2008

Received in revised form

6 July 2008

Accepted 25 July 2008

Communicated by B.A. Korgel

Available online 31 July 2008

### PACS:

81.05.je

81.07.Bc

81.10.Dn

81.16.Be

81.16.Dn

### Keywords:

A1. Crystal morphology

A1. Hierarchical microstructures

A1. Nanostructures

A2. Hydrothermal crystal growth

B1. Oxides

## ABSTRACT

Molybdenum oxide-based hierarchical microstructures assembled radially by anisotropic nanostructures (nanoplates/microprisms/nanorods) have been synthesized at low temperatures for the first time via a facile template-free hydrothermal approach. The influence of hydrothermal temperature, time, concentration of the peroxomolybdic acid solution, and additives on the morphology of products has been investigated. It has been found that the morphology of urchin-shaped microstructures of peroxo-modified molybdenum oxide hydrates can be controlled in the temperature range of 65–75 °C. The as-synthesized uniform microstructures, which are collected from the 0.9 mol/L molybdenum solutions after 14 h at 75 °C, are 35–40 μm in diameter, and they are constructed by nanoscale blocks of 300–400 nm in width and ~190 nm in thickness. The dimensions of microstructures and their building blocks are dramatically magnified when the molybdenum concentration is reduced, while those dimensions can be efficiently decreased by adding small quantities of HNO<sub>3</sub> or LiNO<sub>3</sub> into the precursor solution. By moderate calcination, α-MoO<sub>3</sub> with a hierarchical microstructure can be achieved. The possible formation mechanism of urchin-shaped microstructures is discussed using the results of UV–visible spectroscopy and electron microscopy.

© 2008 Elsevier B.V. All rights reserved.

## 1. Introduction

In recent years, hierarchical microstructures assembled by nanoscale anisotropic building blocks (nanotubes, nanowires, nanorods, and nanobelts) have attracted considerable attention because they are expected to display superior performances as functional nanodevices [1–4]. Various oxides with hierarchical structures, such as MnO<sub>2</sub> [5–8], ZnO [9–11], and others [12–16], have been successfully synthesized, and novel optical, electrical, and magnetic properties have been demonstrated.

Among the anisotropic materials, molybdenum oxides, especially α-MoO<sub>3</sub>, have attracted much attention and have been used as active components in catalysts [17], gas sensors [18], electrochemical cathodes [19], and field emitters [20,21]. Furthermore, their performances strongly depend on specific microstructure morphologies [17–19,21]. For these reasons, substantial efforts have been focused on the controllable synthesis of molybdenum

oxide-based hierarchical microstructures. One-dimensional nanoscale arrays have been made available by physical methods [21–26] and hard template/host methods [27,28]. In the hydrothermal synthesis above 120 °C, molybdenum oxides form fascinating morphologies, such as bundles of nanofilaments [29] and multilamellar nanofibers [30], using organic templates. Recently, flowerlike hierarchical structures have been fabricated in the presence of cetyltrimethylammonium bromide in the hydrothermal process at 180 °C [31]. On the other hand, crosslike nanoflowers have been observed at 180 °C without the need for a template [32]. However, it is still a challenge to organize the nanoscale anisotropic molybdenum oxides into hierarchical structures at low temperatures.

In previous studies of Qian et al. [33] and our group [34], discrete anisotropic α-MoO<sub>3</sub> nanostructures have been achieved under high-temperature hydrothermal conditions. In this paper, for the first time we present the low-temperature synthesis of molybdenum oxide-based hierarchical structures without the need for a template. Spherical radial assemblies based on nanoplates/microprisms/nanorods have been prepared using peroxomolybdic acid. The effects of the hydrothermal synthesis

\* Corresponding author. Tel.: +86 411 84379015; fax: +86 411 84691570.  
E-mail address: taozhang@dicp.ac.cn (T. Zhang).

parameters (temperature, time, concentration, and acid/neutral additives) on the morphology of the building blocks and microstructures are addressed systematically.

## 2. Experimental section

### 2.1. Synthesis

Ammonium heptamolybdenum tetrahydrate (AHM;  $(\text{NH}_4)_6\text{Mo}_7\text{O}_{24} \cdot 4\text{H}_2\text{O}$ , 99.0%, Tianjin KAIDA Chemical Plant), 30% aqueous hydrogen peroxide ( $\text{H}_2\text{O}_2$ , AR, Shanghai Yuanda Peroxide Limited Company), concentrated nitric acid ( $\text{HNO}_3$ , AR, 15 mol/L, Shenyang Chemical Reagent Factory), and lithium nitrate ( $\text{LiNO}_3$ , AR, Tianjin Kernel Chemical Reagent Development Center) were used as received. In a typical procedure, AHM was calcined at  $500^\circ\text{C}$  for 4 h to obtain bulk  $\text{MoO}_3$  powder. The bulk  $\text{MoO}_3$  powder (1.44 g) was added to 30% aqueous  $\text{H}_2\text{O}_2$  (11 mL) and dissolved completely after stirring for 6 h at  $30^\circ\text{C}$ , forming the transparent yellow-green peroxomolybdic acid solution (mother liquor, the molybdenum concentration is 0.9 mol/L). In some control experiments, the additive (deionized water, concentrated  $\text{HNO}_3$ , or  $\text{LiNO}_3$ ) was added together with the bulk  $\text{MoO}_3$  powder into the synthesis system. The resultant precursor solution was transferred into a 20 ml Teflon-lined stainless steel autoclave. The autoclave was then sealed, immersed completely in a thermostatic water bath, and maintained at  $60\text{--}75^\circ\text{C}$  for 8–45 h. The temperature was controlled by a Beckman temperature controller and determined by a thermometer with a scale resolution of  $0.5^\circ\text{C}$ . After cooling in ambience, the solid product was filtered, rinsed with deionized water, and dried at  $40^\circ\text{C}$ .

### 2.2. Characterization

The obtained products were characterized by X-ray powder diffraction (XRD, Rigaku D/max-RB X-ray diffractometer with graphite-monochromatized  $\text{Cu K}\alpha$  radiation), scanning electron microscopy (SEM, JEOL JSM-6360LV), transmission electron microscopy (TEM, JEOL JEM-2000EX microscope), thermogravimetric analysis (TG, Shimadzu Thermal Analyzer DT-20B), temperature programmed decomposition-mass spectrometry (TPDE-MS, Omnistar GSD 301 O3 mass spectrometer), Fourier transform infrared spectrometry (FTIR, Bruker Equinox 55), and  $\text{N}_2$  adsorption ( $-196^\circ\text{C}$ , Micromeritics ASAP 2010, Brunauer–Emmett–Teller method).

The diluted mother liquor, intermediate liquid samples, and the solid product were also examined with UV–visible spectrometry (Cintra 20 double beam UV–visible spectrometer, GBC scientific equipment PTY LTD).  $\text{BaSO}_4$  was used as the reference in diffuse reflectance spectroscopy.

## 3. Results and discussion

### 3.1. Formation of molybdenum oxide-based hierarchical microstructures at different temperatures

It was previously found that only discrete  $\alpha$ -molybdenum trioxide nanorods/nanobelts without hierarchical structures could be obtained under high-temperature hydrothermal conditions [33,34]. However, when the hydrothermal temperature was lowered to  $75^\circ\text{C}$ , well-defined hierarchical microstructures assembled radially by nanostructures were observed on a large scale. Furthermore, both the morphology of the hierarchical microspheres and their building blocks showed strong dependence on the hydrothermal temperature.

When the hydrothermal treatment proceeded at  $60^\circ\text{C}$  for 45 h with the 0.9 mol/L molybdenum solution, no solid product was obtained, while the color of the solution changed from yellow-green to deep orange-red. When the temperature was increased to 65, 70, and  $75^\circ\text{C}$ , a yellow solid product and yellow-green liquid were simultaneously obtained after 45 h. Under these conditions, samples were prepared in a strong oxidative environment created by the addition of excess  $\text{H}_2\text{O}_2$ . It can therefore be assumed that the oxidation state for molybdenum keeps the highest valence, VI, during the entire process. Considering the aqueous environment and strong coordination capacity of the peroxy groups with molybdenum (VI), a nominal formula of  $\text{MoO}_{3-x}(\text{O}_2)_x \cdot y\text{H}_2\text{O}$  ( $0 < x < 1$ ) can be assigned to these resultant samples. The XRD patterns of the solid products were similar to that of  $\alpha\text{-MoO}_3 \cdot \text{H}_2\text{O}$  (triclinic system, space group  $P\bar{1}$ , JCPDS card no. 26-1449) for definite forms of molybdenum-based compounds. Their diffraction peaks were broad and some of them had a certain deviation of  $d$  values, as shown in Fig. 1a. Via a moderate temperature programmed decomposition reaction in a nitrogen atmosphere,  $\text{MoO}_3$  can eventually be obtained. Thus, the total content of the peroxy groups and water of crystallization in the resultant samples could be obtained by TG, and the content of the corresponding peroxy groups could be determined by TPDE-MS. Through the above determination, the compounds obtained at 65, 70, and  $75^\circ\text{C}$  had the nominal formulas  $\text{MoO}_{2.68}(\text{O}_2)_{0.32} \cdot 0.91\text{H}_2\text{O}$ ,  $\text{MoO}_{2.76}(\text{O}_2)_{0.24} \cdot 0.97\text{H}_2\text{O}$ , and  $\text{MoO}_{2.74}(\text{O}_2)_{0.26} \cdot 0.93\text{H}_2\text{O}$ , respectively. This implied that the ratio of peroxy groups to molybdenum in our samples was 0.25–0.33. In addition, it was speculated that the peroxy groups coordinated with molybdenum according to the previous reports [35–37].

The typical crystal morphologies of the as-synthesized samples at 65, 70, and  $75^\circ\text{C}$  are shown in Fig. 2. The low-magnification SEM images of the sample obtained at  $65^\circ\text{C}$  (Fig. 2a and b) clearly showed that there existed a great number of microspheres with diameters from 25 to  $45\ \mu\text{m}$ , and the individual particles were not very regular in shape. The high-magnification SEM images (Fig. 2c–e) revealed that these spherical structures were assembled by numerous nanoplates, which were 70–95 nm in thickness and  $\sim 900$  nm in width. These high-density nanoplates pointed outward from the center of the sphere. Most of them presented sharp tips and rough edges. The sectional images observed occasionally indicated that these microspheres were solid (Fig. S1) and closely joined one another (Fig. 2a and b and S1). This interconnection could primarily be attributed to low fluid convection at low temperatures and low mobility of the

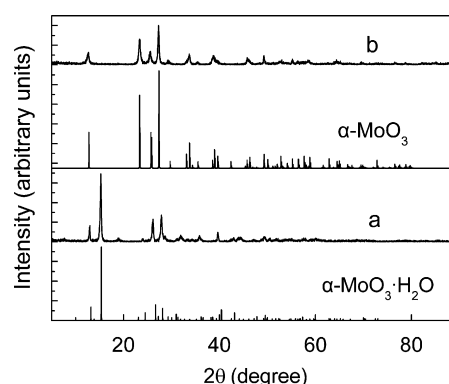
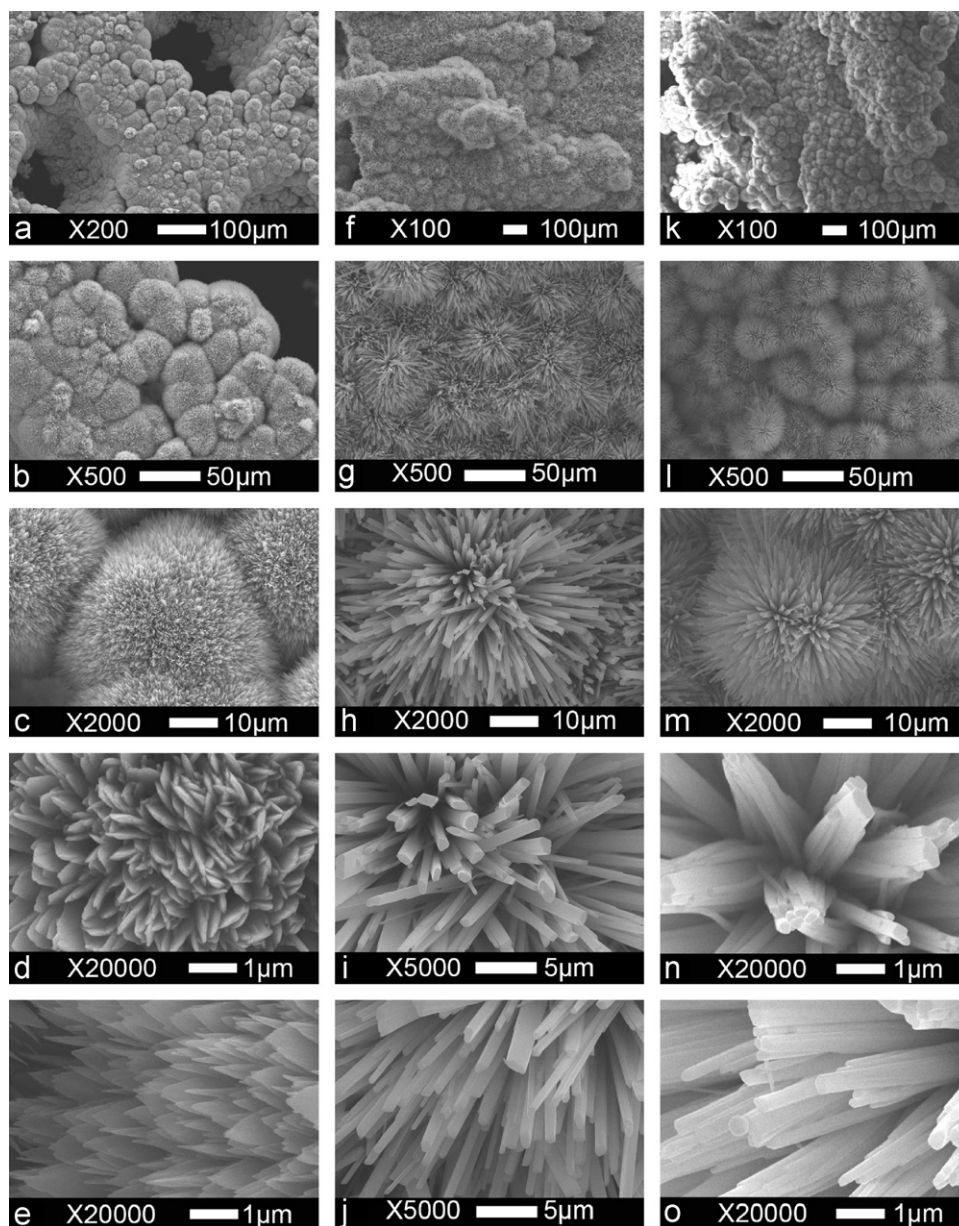


Fig. 1. XRD patterns of solid products (a) prepared from the 0.9 mol/L molybdenum solution for 45 h at the hydrothermal temperature of  $75^\circ\text{C}$ ; (b) obtained after calcination of the sample (a) in air at  $250^\circ\text{C}$  for 2 h.



**Fig. 2.** SEM images of solid products which were prepared from the 0.9 mol/L molybdenum solution for 45 h at different hydrothermal temperatures: (a–e) 65 °C, (f–j) 70 °C, and (k–o) 75 °C.

microspheres [12]. When the temperature was increased to 70 °C, the sample exhibited microspheres with diameters from 50 to 55 μm (Fig. 2f and g) and individual urchin-shaped particles became more regular. Moreover, the high-magnification SEM images (Fig. 2h–j) showed that these radial microstructures were constructed by many microprisms, which were ~850 nm in thickness, 1.4 μm in width, and had irregular rectangular cross-sections. Most of the microprisms showed flat tops and smoothed rims. When the temperature was further raised to 75 °C, microspheres 35–40 μm in diameter were displayed (Fig. 2k and l). The high-magnification SEM images (Fig. 2m–o) showed that these regular radiate particles were fabricated by a substantial number of nanorods, which were 300–400 nm in width and ~190 nm in thickness. Nanorods with flat ends and smoothed edges displayed constant width/thickness along their length. In most regions, parallel nanorods agglomerated to bundles and even thickened into larger rods.

### 3.2. Formation of molybdenum oxide-based hierarchical microstructures at different times

To trace the growth process of the molybdenum oxide-based hierarchical microstructures, we investigated the time dependence of the morphology of microstructures and the corresponding building blocks in the hydrothermal process. In this process the temperature was fixed at 75 °C. Before the formation of the molybdenum oxide-based material, there was an induction period during which no solid product could be seen, but the color of the solution changed gradually from yellow-green (Fig. 3a) to deep orange-red (Fig. 3b). When the time proceeded to 10 h, a solid product which was adhering to the liner began to emerge. The solid product increased gradually with time and reached 1.11 g at 45 h (the yield was 67%). Because the solid product emerged first on the Teflon liner, Teflon slides were put in the precursor solution to act as a substrate to collect the product. The samples along with

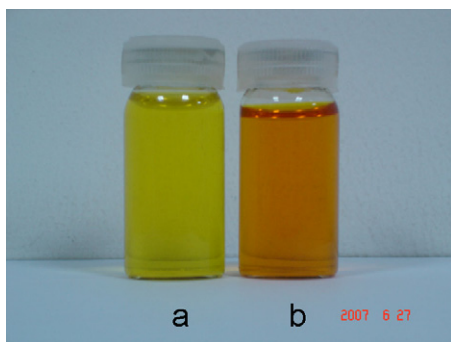


**Fig. 3.** Change in color of the solution: (a) yellow-green mother liquor and (b) deep orange-red intermediate solution.

the Teflon slides were directly used in SEM characterization without the destruction of morphology.

Fig. 4 shows the morphological changes of samples as the hydrothermal time increased. When the time was 10 h, microspheres with diameters of  $\sim 10 \mu\text{m}$  were collected, but the urchin shape was irregular (part I in Fig. 4a; Fig. 4b). The high-magnification SEM images (Fig. 4c–e) showed that these microstructures were constructed radially of numerous nanoplates/nanorods, which were  $\sim 50 \text{ nm}$  in thickness,  $\sim 180 \text{ nm}$  in width, and possessed sharp tips. It should be pointed out that in Fig. 4a some irregular compressed microstructures (part II in Fig. 4a) were adhering to the Teflon slide (part III in Fig. 4a). Their diameters were  $20\text{--}30 \mu\text{m}$ , but their building blocks (Fig. S2) were similar to those of the microspheres (Fig. 4c–e). These compressed microstructures might result from the heterogeneous nucleation and growth, which were due to the high nucleation potential in our experimental system.

When the time was extended to 12 h, the number of microspheres increased quickly, and their diameters were enhanced moderately to  $\sim 15 \mu\text{m}$  (Fig. 4f and g). The urchin shape became more regular. The nanoplates/nanorods building blocks thickened slightly to  $80 \text{ nm}$ , widened to  $400 \text{ nm}$ , and still presented sharp tips (Fig. 4h–j). When the time was prolonged to 14 h, the microspheres increased quickly to  $30 \mu\text{m}$  in diameter (Fig. 4k and l). Uniform microspheres were manufactured by straight nanorods which were  $\sim 150 \text{ nm}$  in thickness and  $400 \text{ nm}$  in width (Fig. 4m–o). The top of most nanorods became flat. During the time range of 14–45 h, building blocks of microspheres grew slowly on account of the decreased concentration of the solution and the steric restraint effect. The above results suggested that the morphology of microspheres and their building blocks could be modestly adjusted by controlling the hydrothermal time.

### 3.3. Formation of molybdenum oxide-based hierarchical microstructures at different concentrations

The influence of the concentrations of peroxomolybdic acid solutions on morphologies of products was subsequently explored. When the mother liquor was diluted to  $0.45 \text{ mol/L}$  with the deionized water, it was found that the diameters of the microspheres increased dramatically from  $35$  to  $220 \mu\text{m}$  (Fig. 5a and b), and the interconnection between them weakened. Uniform intact particles consisted of numerous submicrometer rods, which were  $\sim 600 \text{ nm}$  in thickness and  $1.5 \mu\text{m}$  in width. Most of the submicrometer rods had irregular shapes in cross-sections, flat tops, and clear edges (Fig. 5c and d). When the mother liquor was further diluted to  $0.2 \text{ mol/L}$ , there were only several sparse particles visible. These loose microspheres,  $350\text{--}400 \mu\text{m}$  in diameter, were constructed by rods  $400\text{--}500 \text{ nm}$  in width/

thickness (Fig. 5e–h). The above results indicated that decreasing the concentration of peroxomolybdic acid in the precursor solution strongly inhibited the nucleation, and thus the molybdenum oxide-based materials could grow sufficiently during the hydrothermal process due to the weakened steric restraint.

### 3.4. Formation of molybdenum oxide-based hierarchical microstructures in the presence of additives

As mentioned above, the molybdenum oxide-based hierarchical microspheres obtained from the pure peroxomolybdic acid solution were interconnected. In an attempt to obtain the discrete microstructures, we utilized two additives to facilitate the nucleation, and then investigated the influence of additives on the morphology. One additive selected was  $\text{HNO}_3$  since protons are involved in the synthesis system and may change the equilibrium of the reaction network. The other additive used to compare the effects of the cations on the morphology was  $\text{LiNO}_3$ . According to the literature, lithium salts cannot affect the crystal structures of molybdenum oxides [38,39].

When  $0.1 \text{ ml}$  concentrated  $\text{HNO}_3$  was added into the mother liquor ( $\text{H}_{\text{add}}^+/\text{Mo} = 0.15$ ), the resultant mixture was comprised of the suspended slurry and the solid product adhering closely to the liner. The microstructures in the suspended slurry were discrete and shrank dramatically to  $\sim 20 \mu\text{m}$  in diameter (Fig. 6a and b), compared to the joined microstructures with  $35 \mu\text{m}$  in diameter obtained without the additive. These urchin-shaped microstructures were assembled by nanorods which were  $\sim 200 \text{ nm}$  in width,  $130 \text{ nm}$  in thickness, and had flat ends (Fig. 6c–e). To observe the solid product adhering closely to the liner, a Teflon slide had been put into the solution as a substrate to collect the product. Some closely interconnected microstructures (part I in Fig. S3) adhered to the Teflon slide (part II in Fig. S3), and their building blocks (Fig. S3) were similar to those of the microspheres in the slurry (Fig. 6c–e). When the acid was added, on one hand, protons could combine with the anionic molybdenum species, and stimulate the production of the molybdenum oxide hydrates. Thus, the nucleation in the solution was favored and discrete microspheres could be collected in the slurry. On the other hand, the acid could stabilize the peroxy groups in the molybdenum species and then increase the nucleation potential. Consequently, the molybdenum species was compelled to nucleate on the surface of the substrate (Teflon slide and liner). As more acid was added, the adhering structure became the major component in the solid product.

In comparison to the products obtained from the addition of  $\text{HNO}_3$ , only the suspended slurry could be obtained when  $0.10 \text{ g}$   $\text{LiNO}_3$  was added to the mother liquor ( $\text{Li}_{\text{add}}^+/\text{Mo} = 0.15$ ). The discrete microstructures in the suspended slurry were comparable with the sample using the acid additive, i.e.,  $\sim 20 \mu\text{m}$  in diameter (Fig. 6f and g), but they were constructed by smaller nanorods  $\sim 100 \text{ nm}$  in width/thickness. Moreover, it was very surprising that these nanorods had acicular ends in contrast to the flat-topped nanorods obtained in the presence of  $\text{HNO}_3$  (Fig. 6h–j). As more  $\text{LiNO}_3$  was added, the hierarchical microstructures were gradually destroyed. When the amount of  $\text{LiNO}_3$  was increased to  $0.69 \text{ g}$  ( $\text{Li}_{\text{add}}^+/\text{Mo} = 1$ ), the urchin-shaped morphology vanished, but the anisotropic morphology still remained (Fig. 6k and l).

We failed to obtain the discrete hierarchical microstructures by treating an interconnected sample with ultrasonication. Isolated nanorods of peroxy-containing molybdenum oxide hydrates ( $2\text{--}5 \mu\text{m}$  in length) were obtained after the treatment under  $25\text{--}35^\circ\text{C}$  for 5 h (Fig. S4). It turned out that not only could the hierarchical microstructure be separated into discrete nanorods under violent agitation, but the nanoscale building blocks could be broken irregularly by ultrasonication. The morphology of these discrete nanorods was similar to that of the isolated  $\alpha\text{-MoO}_3 \cdot \text{H}_2\text{O}$

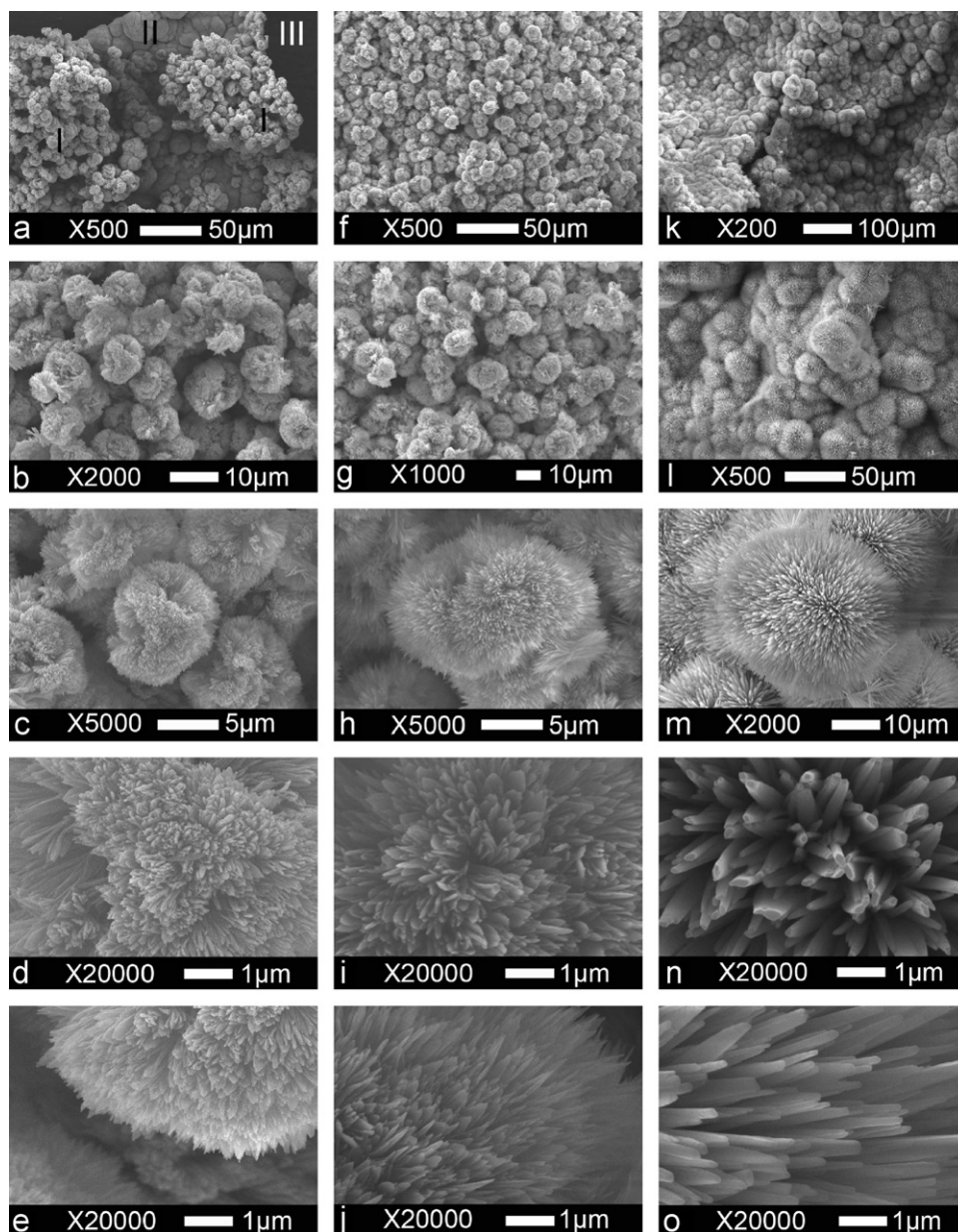


**Fig. 4.** SEM images of solid products which were prepared from the 0.9 mol/L molybdenum solution at 75 °C for different times: (a–e) 10 h, (f–j) 12 h, and (k–o) 14 h.

nanorods directly obtained from the peroxomolybdic acid solution under ultrasound irradiation [40].

The aforementioned results demonstrated that the discrete molybdenum oxide-based hierarchical microstructures could be achieved by a slight enhancement of the ionic concentration, and their dimensions could be decreased remarkably by this facile modified synthesis.

### 3.5. Characterization of $\alpha$ -MoO<sub>3</sub> hierarchical microstructures

To investigate whether molybdenum oxide-based materials can transform thermally to  $\alpha$ -MoO<sub>3</sub> without damaging the original hierarchical microstructures, a typical sample of molybdenum oxide-based material, which was synthesized from the 0.9 mol/L molybdenum solution at 75 °C for 45 h, was calcined in air at 250 °C for 2 h. After this moderate calcination, the characteristic XRD peaks of peroxo-modified molybdenum oxide hydrate vanished and those of  $\alpha$ -MoO<sub>3</sub> appeared (orthorhombic

system, space group *Pbnm*, JCPDS card no. 35-0609) (Fig. 1b). In our previous study, it was found that the XRD pattern of  $\alpha$ -MoO<sub>3</sub> obtained directly at a higher hydrothermal temperature displayed an intensity ratio different from the JCPDS data due to its strong preferred orientation [34]. However, it was noted that the XRD pattern of the sample after calcination presented an intensity ratio similar to the JCPDS data. The IR spectrum of the calcined sample was in good accordance with the typical spectrum of  $\alpha$ -MoO<sub>3</sub> (Fig. S5) [41]. Moreover, after calcination, the BET surface area increased slightly from 8.3 to 11.7 m<sup>2</sup>/g due to the decomposition of peroxo-modified molybdenum oxide hydrate. It was noted that for  $\alpha$ -MoO<sub>3</sub> the surface area of the hierarchical microstructure is higher than that of bulk powder obtained from the direct calcination of AHM (2.4 m<sup>2</sup>/g), and is comparable with that of nanorods (13.4 m<sup>2</sup>/g) [38]. Nevertheless, this surface area is smaller than those of nanofibers (35 m<sup>2</sup>/g) [29] and nanowhiskers (55.4 m<sup>2</sup>/g) [40]. From the SEM images (Fig. S6), it was clear that the morphology of the hierarchical microstructures and their

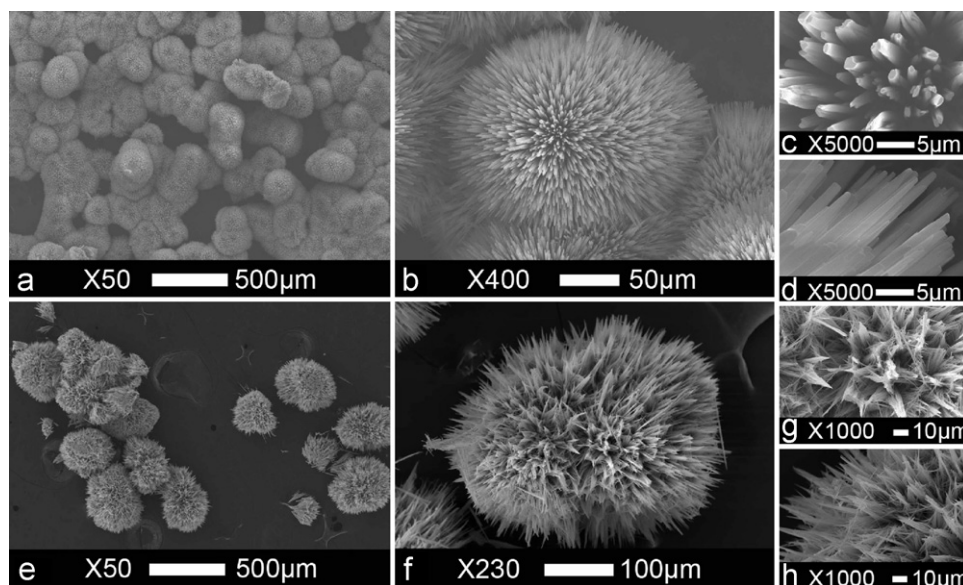


Fig. 5. SEM images of solid products which were prepared from different concentrations of molybdenum solutions diluted with deionized water at 75 °C for 45 h: (a–d) the 0.45 mol/L molybdenum solution; (e–h) the 0.2 mol/L molybdenum solution.

building blocks were essentially preserved after the calcination. Thus, the pure  $\alpha$ - $\text{MoO}_3$  hierarchical microstructures could be successfully synthesized by the hydrothermal calcination process, and present a promising potential for catalytic, electrical, and electrochemical applications.

### 3.6. The possible mechanism of the formation of hierarchical microstructures

The results in Section 3.2 demonstrated that the morphology of hierarchical microstructures showed a strong dependence on hydrothermal time. Particularly, it was interesting that during the long induction period the color of the solution changed apparently from yellow-green (Fig. 3a) to deep orange-red (Fig. 3b), which may imply the transformation of species in the solution and may reveal the key step in determining the distinctive morphology. Thus, we conducted UV–visible spectrometric analyses to investigate the configurations of species in the solutions (Fig. 7).

Both the mother liquor (Fig. 3a) and the intermediate solution (Fig. 3b) could completely absorb the light below 350 nm due to their high concentration (0.9 mol/L). Therefore, they were diluted to  $\sim 0.1$  mmol/L to distinguish the two spectra. Both of the two liquid samples (Fig. 7a and b) presented the broad absorption bands centered at 230 and 310 nm, which could be attributed to the charge transfer transitions of the characteristic heptacoordination in the peroxomolybdic acid species (from  $\text{O}^{2-}$  to Mo(VI), and from  $\text{O}_2^{2-}$  to Mo(VI)) [37]. However, a strong absorption at 213 nm could be observed only in the spectrum of the diluted intermediate solution (Fig. 7b). This adsorption band might correspond to the coexistence of octahedral and tetrahedral molybdenum species, because both of these two typical species demonstrate the band around 210 nm in absorption spectra [42]. Compared with this adsorption band, the absorption at 210 and 264 nm could also be observed in the diffuse reflectance spectra of the yellow solid product (Fig. 7c), which are associated with the octahedral and tetrahedral coordination of molybdenum species [37,43]. Based on the similarity of the absorption band at 210 nm, it could be suggested that at the end of the induction period the characteristic structural units in the intermediate solution (octahedral and tetrahedral species) were very similar to those in the solid product obtained subsequently. In the yellow solid

product, the additional band at 375 nm corresponds primarily to the absorption of the tetrahedral coordination of molybdenum species resulting from the peroxo-modified structure [43].

The UV–visible results revealed the evolution of molybdenum species in the solution. As the color of the solution changed from yellow-green to deep orange-red, the monomeric and/or dimeric molybdenum species which formed at the high peroxide concentration condensed to low-condensed species. Moreover, the characteristic structural units (octahedral and tetrahedral molybdenum species) emerged. As time progressed, these units evolved into the building blocks of peroxo-modified  $\alpha$ - $\text{MoO}_3 \cdot \text{H}_2\text{O}$ .

The subsequent morphological evolution of the solid samples could be observed from the SEM results in Section 3.2. Two stages existed in the formation process of the hierarchical microstructures. Initially, nanoscale building blocks agglomerated spontaneously and radially into the incipient microstructures. As time proceeded, kinetically controlled growth instead of agglomeration became dominant. Fig. 6m shows the low-magnification TEM image of a typical region of a product. Combined with the high-magnification TEM image (Fig. 6n), the selected area electron diffraction pattern (SAED, inset of Fig. 6n) indicated that the single-crystal building block grew along the [001] orientation. This result could be interpreted as follows. The resultant peroxo-modified  $\alpha$ - $\text{MoO}_3 \cdot \text{H}_2\text{O}$  might keep the isolated double-chain configuration along the [001] axis, and these chains are linked together by weak hydrogen bonding in  $\alpha$ - $\text{MoO}_3 \cdot \text{H}_2\text{O}$  [44]. From the viewpoint of energy, the growth along the [001] axis could be favorable during the kinetically controlled growth stage, furthering the anisotropic growth along the length of the building blocks. Therefore, the specific radial agglomeration and the growth determined by the intrinsic crystal structure led to the final urchin-shaped hierarchical microstructures.

## 4. Conclusions

For the first time, under the low temperature of 65–75 °C molybdenum oxide-based hierarchical microstructures, assembled radially by anisotropic nanostructures (nanoplates/microprisms/nanorods), have been controllably synthesized without the need for a template. The hydrothermal temperature, time,

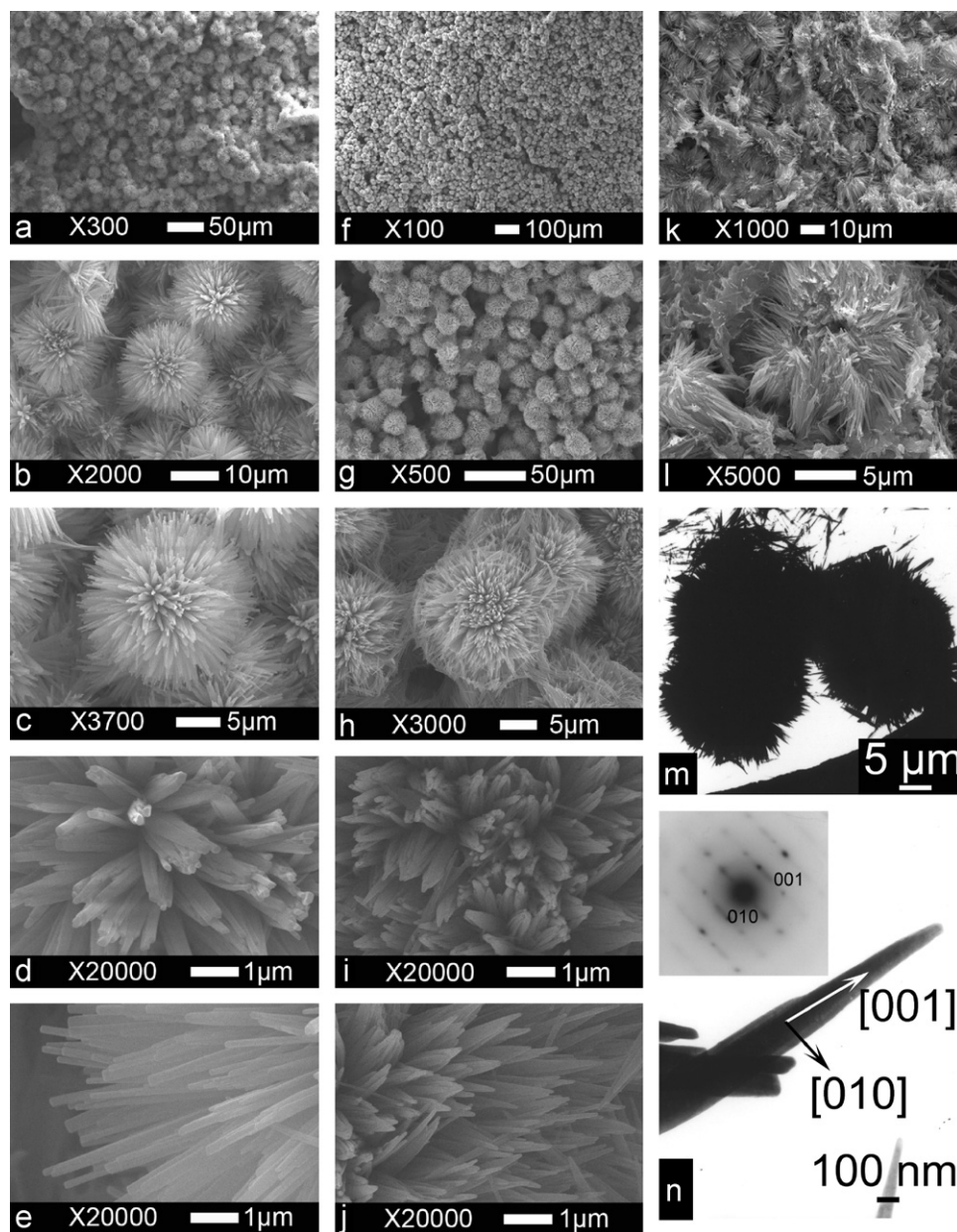


**Fig. 6.** Images of solid products prepared from the 0.9 mol/L molybdenum solution in the presence of additives at 75 °C for 45 h. In the precursor solution, concentrations of additives and types of images are (a–e) 0.14 mol/L HNO<sub>3</sub>, SEM images, (f–j) 0.14 mol/L LiNO<sub>3</sub>, SEM images, (k–l) 0.91 mol/L LiNO<sub>3</sub>, SEM images, and (m–n) 0.14 mol/L LiNO<sub>3</sub>, TEM images; the inset of (n): the SAED.

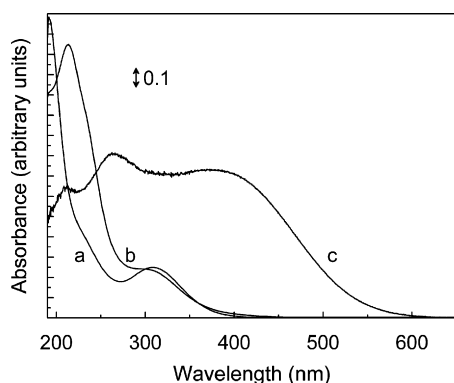


**Fig. 7.** UV-visible spectra of the samples: (a) diluted mother liquor, (b) diluted intermediate solution, and (c) yellow solid product.

concentration of the peroxomolybdic acid solution, and additives are the key factors in controlling the morphology of the products and their building blocks. When the molybdenum concentration is 0.9 mol/L in the precursor solution, urchin-shaped microstructures with diameters of 35–40 μm are fabricated by uniform nanoscale blocks (300–400 nm in width and ~190 nm in thickness) after 14 h at 75 °C. Diameters of the spherical microstructures can be tuned efficiently from 20 to 400 μm by varying the ionic strength and the concentration of molybdenum in the precursor solution. Furthermore, pure α-MoO<sub>3</sub> with hierarchical microstructures can be synthesized after moderate calcination. Thus, molybdenum oxide-based hierarchical materials obtained by this approach can be considered as a promising candidate for catalytic, electrical, and electrochemical applications. This study provides an advantageous and novel process for the synthesis of transition metal oxides with hierarchical microstructures.

## Acknowledgments

This work was supported by the National Natural Science Foundation of China for Distinguished Young Investigators (No. 20325620). We gratefully acknowledge Dr. Xingyun Huang for the XRD experiments and Dr. Xiu-Ying Gao for the TG examination. Liang Fang acknowledges Dr. Yuning Li for her kind help in helpful discussions and grammar check.

## Appendix A. Supplementary materials

The online version of this article contains additional supplementary data. Please visit [doi:10.1016/j.jcrysgro.2008.7.080](https://doi.org/10.1016/j.jcrysgro.2008.7.080)

## References

- [1] G.R. Patzke, F. Krumeich, R. Nesper, *Angew. Chem. Int. Ed.* 41 (2002) 2446.
- [2] Y. Huang, X.F. Duan, Q.Q. Wei, C.M. Lieber, *Science* 291 (2001) 630.
- [3] B. Messer, J.H. Song, P.D. Yang, *J. Am. Chem. Soc.* 122 (2000) 10232.
- [4] Y.Y. Wu, H.Q. Yan, M. Huang, B. Messer, J.H. Song, P.D. Yang, *Chem. Eur. J.* 8 (2002) 1261.
- [5] C.Z. Wu, Y. Xie, D. Wang, J. Yang, T.W. Li, *J. Phys. Chem. B* 107 (2003) 13583.
- [6] Z.Q. Li, Y. Ding, Y.J. Xiong, Q. Yang, Y. Xie, *Chem. Commun.* (2005) 918.
- [7] J.K. Yuan, W.N. Li, S. Gomez, S.L. Suib, *J. Am. Chem. Soc.* 127 (2005) 14184.
- [8] B. Tang, G.L. Wang, L.H. Zhuo, J.C. Ge, *Nanotechnology* 17 (2006) 947.
- [9] M.S. Mo, J.C. Yu, L.Z. Zhang, S.K.A. Li, *Adv. Mater.* 17 (2005) 756.
- [10] H. Zhang, D.R. Yang, Y.J. Ji, X.Y. Ma, J. Xu, D.L. Que, *J. Phys. Chem. B* 108 (2004) 3955.
- [11] B. Liu, H.C. Zeng, *J. Am. Chem. Soc.* 126 (2004) 16744.
- [12] B. Liu, H.C. Zeng, *J. Am. Chem. Soc.* 126 (2004) 8124.
- [13] C. O'Dwyer, D. Navas, V. Lavayen, E. Benavente, M.A. Santa Ana, G. González, S.B. Newcomb, C.M.S. Torres, *Chem. Mater.* 18 (2006) 3016.
- [14] Y.B. Mao, M. Kanungo, T. Hemraj-Benny, S.S. Wong, *J. Phys. Chem. B* 110 (2006) 702.
- [15] Z.J. Gu, T.Y. Zhai, B.F. Gao, X.H. Sheng, Y.B. Wang, H.B. Fu, Y. Ma, J.N. Yao, *J. Phys. Chem. B* 110 (2006) 23829.
- [16] A. Michailovski, F. Krumeich, G.R. Patzke, *Chem. Mater.* 16 (2004) 1433.
- [17] A. Baiker, P. Dollenmeier, A. Reller, *J. Catal.* 103 (1987) 394.
- [18] A.M. Taurino, A. Forleo, L. Francioso, P. Siciliano, M. Stalder, R. Nesper, *Appl. Phys. Lett.* 88 (2006) 152111.
- [19] W.Y. Li, F.Y. Cheng, Z.L. Tao, J. Chen, *J. Phys. Chem. B* 110 (2006) 119.
- [20] Y.B. Li, Y. Bando, D. Golberg, K. Kurashima, *Appl. Phys. Lett.* 81 (2002) 5048.
- [21] J.G. Liu, Z.J. Zhang, C.Y. Pan, Y. Zhao, X. Su, Y. Zhou, D.P. Yu, *Mater. Lett.* 58 (2004) 3812.
- [22] J. Zhou, N.S. Xu, S.Z. Deng, J. Chen, J.C. She, Z.L. Wang, *Adv. Mater.* 15 (2003) 1835.
- [23] J. Zhou, S.Z. Deng, N.S. Xu, J. Chen, J.C. She, *Appl. Phys. Lett.* 83 (2003) 2653.
- [24] Y.B. Li, Y.S. Bando, *Chem. Phys. Lett.* 364 (2002) 484.
- [25] J. Zhou, N.S. Xu, S.Z. Deng, J. Chen, J.C. She, *Chem. Phys. Lett.* 382 (2003) 443.
- [26] L. Kumari, Y.R. Ma, C.C. Tsai, Y.W. Lin, S.Y. Wu, K.W. Cheng, Y. Liou, *Nanotechnology* 18 (2007) 115717.
- [27] M.P. Zach, K.H. Ng, R.M. Penner, *Science* 290 (2000) 2120.
- [28] F. Wang, Y.L. Zhang, Q.S. Wei, K. Wu, Y.C. Xie, *Acta Phys. Chim. Sin.* 20 (2004) 637.
- [29] M. Niederberger, F. Krumeich, H.J. Muhr, M. Müller, R. Nesper, *J. Mater. Chem.* 11 (2001) 1941.
- [30] R.Q. Song, A.W. Xu, B. Deng, Y.P. Fang, *J. Phys. Chem. B* 109 (2005) 22758.
- [31] S.T. Wang, Y.G. Zhang, X.C. Ma, W.Z. Wang, X.B. Li, Z.D. Zhang, Y.T. Qian, *Solid State Commun.* 136 (2005) 283.
- [32] G.C. Li, L. Jiang, S.P. Pang, H.R. Peng, Z.K. Zhang, *J. Phys. Chem. B* 110 (2006) 24472.
- [33] X.K. Hu, D.K. Ma, L.Q. Xu, Y.C. Zhu, Y.T. Qian, *Chem. Lett.* 35 (2006) 962.
- [34] L. Fang, Y.Y. Shu, A.Q. Wang, T. Zhang, *J. Phys. Chem. C* 111 (2007) 2401.
- [35] C.B. Shoemaker, D.P. Shoemaker, L.V. McAfee, C.W. DeKock, *Acta Crystallogr. C* 41 (1985) 347.
- [36] J.M. Le Carpentier, A. Mitschler, R. Weiss, *Acta Crystallogr. B* 28 (1972) 1288.
- [37] J.Y. Piquemal, J.M. Manoli, P. Beaunier, A. Ensuque, P. Tougne, A.P. Legrand, J.M. Brégeault, *Microporous Mesoporous Mater.* 29 (1999) 291.
- [38] G.R. Patzke, A. Michailovski, F. Krumeich, R. Nesper, J.D. Grunwaldt, A. Baiker, *Chem. Mater.* 16 (2004) 1126.
- [39] A. Michailovski, F. Krumeich, G.R. Patzke, *Helv. Chim. Acta* 87 (2004) 1029.
- [40] C.V. Krishnan, J.L. Chen, C. Burger, B. Chu, *J. Phys. Chem. B* 110 (2006) 20182.
- [41] L. Seguin, M. Figlarz, R. Cavagnat, J.C. Lassègues, *Spectrochim. Acta A* 51 (1995) 1323.
- [42] J.J. Cruywagen, J.B.B. Heyns, *Inorg. Chem.* 26 (1987) 2569.
- [43] K. Segawa, K. Ooga, Y. Kurusu, *Bull. Chem. Soc. Jpn.* 57 (1984) 2721.
- [44] I. Böschen, B. Krebs, *Acta Crystallogr. B* 30 (1974) 1795.